Solar-Terrestrial Physics. 2026, vol. 12, iss. 2, pp. 89–95. DOI: 10.12737/stp-122202610. © 2026 O.P. Zhelenkova, M.V. Khoruzhenko. Published by INFRA-M Academic Publishing House

DOI: 10.12737/stp-122202610
EDN: EWXZFL

Received November 07, 2025
Accepted February 19, 2026

ANALYSIS OF GIANT RADIO SOURCE CANDIDATES BASED ON MULTIWAVELENGTH DATA

O.P. Zhelenkova
Special Astrophysical Observatory RAS, Nizhnij Arkhyz, Russia, zhe@sao.ru

M.V. Khoruzhenko
South Federal University, Rostov-on-Don, Russia, milenka_khoruzenko@mail.ru

Abstract. The NVGRC catalog includes objects selected by the pattern recognition algorithm from the NVSS survey as candidates for giant radio sources (GRS). We have studied in detail 370 NVGRC objects falling within the right ascension interval 00^h00^m–05^h20^m to confirm their GRS classification. The GLEAM, TGSS, RACS, and VLASS radio surveys were used to determine the radio morphology of the NVGRC objects; the LS, DES, UKIDSS, and WISE optical and infrared surveys, to identify their host galaxies; and the VizieR, NED, and NOAO DataLab databases, to determine their redshifts. This work would not have been possible without the information resources and software of the virtual observatory. Of the 370 NVGRC objects examined, 187 radio sources were classified as GRS; 82 of them were previously known as GRS from publications. We have confirmed for the first time that 105 NVGRC objects are GRS. For 98 objects it turned out that their components were not physically connected and were merged into one radio source by a pattern recognition algorithm.

We estimated the efficiency of the algorithm, used for selecting GRS candidates for the NVGRC catalog, at ≈30 %.

Keywords: active galactic nuclei, giant radio sources, astronomical information resources.

INTRODUCTION

Giant radio sources are those with a linear projected radio structure size exceeding 0.7 Mpc. The largest giant radio sources (GRS) have sizes of ~5 Mpc, which is comparable to the size of a galaxy cluster. By 2020, ~900 GRS had been discovered [Dabhade et al., 2020] and they were considered quite rare. To date, more than 11.5 thousand of them are known [Oei et al., 2023; Mostert et al., 2024]. Especially many giants have been found from the LoTSS survey, which is highly sensitive. The LoTSS DR2 survey covers 27 % of the northern sky in two main regions whose centers are located at right ascension of ~13^h and 01^h. Some of our objects fell within the second field of view, namely from 00^h00^m to 02^h49^m in right ascension and from +16°20′ to +43°11′ in declination.

In other sky areas, their detection level remained the same due to the lack of sensitive low-frequency surveys.

Several hypotheses are trying to explain the size of GRS: a less dense intergalactic medium (IGM) in the vicinity of the source [Safouris et al., 2009; Malarecki et al., 2015]; an older age of the radio structure [Kaiser et al., 1997]; special properties of the galactic nucleus [Kuźmicz, Jamrozy, 2012].

Giant radio sources transport matter from the parent galaxy over long distances and enrich IGM with nonthermal particles and magnetic fields [Kronberg, 1994; Oei et al., 2022]. This magnetized plasma can exist for billions of years and serve as a source of injection of high-energy particles into IGM [Enßlin, Gopal-Krishna, 2001; van Weeren et al., 2010].

GRS radio lobes are the largest natural reservoirs of the magnetic field and nonthermal relativistic particles, associated with the galactic system, and store most of the energy, released by black holes, for a long time [Kronberg et al., 2001]. This makes giants an effective tool for estimating the energy released by central black holes. Extended radio lobes of GRS with charged particles are large enough to accelerate particles to extremely high energies. It is assumed that shock waves in jets and GRS lobes can generate cosmic rays [Kronberg et al., 2004; Hardcastle et al., 2009].

The IGM density is rather low near some GRS [Machalski et al., 2006; Malarecki et al., 2015], although no connection between giants and voids has been found [Kuzmicz et al., 2018]. Moreover, Komberg and Pashchenko [2009] have shown that there is no correlation between the size of a radio source and the density of galaxies in its vicinity.

Giant radio sources >4′ in size are of particular interest when separating the radiation of radio sources and the microwave background, as well as when taking into account their contribution to the angular power spectrum used in choosing a cosmological model [Solovyov, Verkhodanov, 2014; Verkhodanov et al., 2016]. Further systematic searches are needed to account for the contribution of GRS to the microwave background throughout the celestial sphere.

In our paper, we have used the NVGRC catalog to search for GRS [Proctor, 2016]. The catalog contains a list of radio sources with angular sizes >4′, which are candidates for GRS, selected from the NVSS catalog by

pattern recognition algorithms. Parent galaxies and redshifts necessary for estimating linear projected sizes of NVGRC catalog objects were not determined by Proctor [2016].

We have carried out a visual inspection of 370 objects, which is a quarter of the sources from the NVGRC catalog. A similar work has previously been done by Dabhade et al. [2017], where parent galaxies were identified only for those radio sources in which a radio core was detected in the VLASS survey. Unlike Dabhade et al. [2017], we have also checked NVGRC objects, whose core is not detected on VLASS maps, to confirm their GRS classification.

In this paper, we adopt the flat cosmology ΛCDM based on the results of the Planck experiment [Aghanim et al., 2020]: H_0=67.4 km s^{-1} Mpc^{-1}, Ω_M=0.315. The radio source spectral index α is defined as $S_\nu \propto \nu^\alpha$.

1. ASTRONOMICAL INFORMATION RESOURCES AND THE RADIO SOURCE INSPECTION METHOD

The NVGRC catalog [Proctor, 2016], we have used in our work, is based on the NVSS catalog [Condon et al., 1998]. The Oblique Classifier One (OC1) software, which implements the decision tree method, was employed to recognize giant radio sources. The OC1 classifiers were configured for a training sample obtained from properties of 48 GRS from [Lara et al., 2001]. As a result, a catalog of 1616 GRS candidates has been compiled. Since the GRS candidates were not verified, along with GRS the catalog contains radio sources smaller than 0.7 Mpc, as well as objects each of two components of which is an independent radio source, but the recognition algorithm merged them into one object. In this regard, it is necessary to verify GRS candidates for their belonging to giants.

Identifying radio sources of large angular size can be quite a challenge. With low surface brightness of radio lobes, it can be difficult to identify the radio source itself and its components. Here we should use maps of both low-frequency and high-frequency radio surveys of different angular resolutions. The former allow us to find extended structures and angular size of a radio source; the latter, to identify a radio core and hot spots, and ultimately to determine the morphology of the radio source.

If a candidate has a radio core that matches an optical object, the identification of the parent galaxy is beyond doubt and will be reliable. But if the radio core is not detected, it is important to identify the radio structure of the source as accurately as possible, and then it will be easier to pinpoint the location of the parent galaxy.

We have additionally employed near- and mid-IR data to identify parent galaxies. Optical or ultraviolet radiation hidden by dust structures around the accretion disk of the active galactic nucleus (AGN) is reradiated in the mid-IR range, whereas the parent galaxy of the radio source usually stands out among other objects. For example, the assumed parent galaxy will be brighter in the K band of the UKIDSS LAS survey or in the W1 and W2 bands of the WISE survey.

We have used the software tools Aladin Sky Atlas [Bonnarel et al., 2000] for working with catalogs and surveys and TOPCAT [Taylor, 2005] for working with Tables.

During the visual inspection of each NVGRC object, we followed a specific sequence of actions. First, coordinates of an object from the NVSS and NVGRC catalogs and the NVSS survey map were loaded into the Aladin stack. To clarify the radio structure, we employed GLEAM, Apertif, RACS-low, RACS-mid, TGSS, FIRST, VLASS, GB6 survey radio maps. In most cases, VLASS maps were used to define the radio morphology.

If there is a radio source core on VLASS maps, the parent galaxy usually coincides with the position of the core. To identify the parent galaxy, we applied optical surveys SDSS [Ahumada et al., 2020], PanSTARRS [Chambers et al., 2016], DES [Abbott et al., 2018], and Legacy Surveys [Dey et al., 2019].

If no radio core was detected in a source, we applied images in the WISE survey bands [Wright et al., 2010]. The object visible in the W1 and W2 bands and well located relative to the radio structure was considered a preferred candidate for parent galaxies.

If two close optical objects were fit for the parent galaxy, we chose a brighter object in the images from near-IR surveys UKIDSS LAS/GPS [Lawrence et al., 2007]. In some cases, in order to distinguish a star from a galaxy by its proper motion or choose a partner for a radio source from two closely spaced optical candidates, we used the Gaia catalog [Vallenari et al., 2023].

Further, in the databases SIMBAD [Wenger et al., 2000], NED [Helou et al., 1995], NOIRDatalab [Olsen et al., 2019], and VizieR [Ochsenbein et al., 2000], we searched for a spectroscopic or photometric redshift of the parent galaxy to estimate the projected linear size of the NVGRC object.

We considered the two components of the NVGRC object to be unrelated if each component was identified with a separate parent galaxy.

2. MEASURING ANGULAR SIZES OF GRS CANDIDATES

To measure angular sizes of radio sources, we have employed NVSS survey maps, as in [Proctor, 2016]. According to the classification proposed by Fanaroff and Riley [1974], the FRI type includes radio sources with brightness decreasing toward the edges; and the FRII type, those with brightening toward the edges. Sources that exhibit signs of both FRI and FRII are now classified as hybrid (FRI/FRII).

The angular size of FRII sources is usually measured as the distance between hot spots. Measurement uncertainties arise mainly in the case of FRI and FRI/FRII sources. The angular size of such objects is determined from the maximum angular distance between edges of radio lobes, where the “edge” of the source is found from the signal-to-noise ratio. For sources with a curved structure, their angular sizes are measured from the source “ridge” [Kuzmicz et al., 2018].

Proctor [2016] estimated angular sizes of FRI, FRII, and hybrid sources along the edge of radio lobes at a level ≈3σ above the background. We have followed the same method.

We compared the projected sizes of GRS from our sample with the same sizes given by Kuzcmicz et al. [2018], Dabhade et al. [2020], and Oei et al. [2023] if such information was available.

The comparison results are presented in Table 1. The first column displays lists of GRS between which the difference in projected linear sizes is calculated. The following designations are used: D20 — [Dabhade et al., 2020], K18 — [Kuzmicz et al., 2018], O23 — [Oei et al., 2023], and OL — our list. The second column shows the number of sources that match in the compared lists. The third column illustrates the average difference between linear sizes and the standard deviation in Mpc.

Table 1

Differences in certain projected linear sizes for known GRS included in our sample

Compared lists	Number of objects	$\Delta D \pm RMS$
K18-D20	257	0.05±0.35
O23-K18	19	0.20±0.28
OL-O23	7	0.18±0.21
OL-D20	51	0.29±0.63
OL-K18	24	0.29±0.18

The systematic difference 0.2–0.3 Mpc between our linear size estimates and the values obtained by Kuzmicz et al. [2018], Dabhade et al. [2020], and Oei et al. [2023] is most likely due to the fact that we measured the angular distance not between hot spots, but along the edges of radio lobes.

3. PARENT OBJECT TYPES

The NVGRC catalog included double radio sources with an angular size of at least 4′. High angular resolution of radio maps is extremely important for reliable identification of the parent galaxy. We have used VLASS survey data (2.5" angular resolution), which allows us to clearly distinguish the radio source structure and pinpoint the location of the radio core, as well as to identify the lobes that are symmetric about the core. This morphology is typical of active radio galaxies and radio quasars. In contrast, the radio emission from nebulae, pulsars, young and active stars usually has an amorphous structure, which makes it possible to reliably distinguish them from radio galaxies. Exceptions are rare and generally associated with insufficient detail of radio maps.

To confirm the correctness of the identification, we have additionally applied deep surveys in the optical and IR ranges, as well as data on color indices of optical candidates and parameters of photometric profiles of potential parent objects from the catalogs.

Eighteen sources from our sample are located in the sky areas close to the galaxy plane with high stellar density. Five of them are already known as GRS from previously published data, and the remaining 13 exhibit morphology typical of radio galaxies. The combination of morphological and photometric features allows us to confidently attribute our sample of GRS to extragalactic objects — galaxies or quasars.

To determine the parent object type, we used information from the SIMBAD, NED, VizieR, SDSS, and LS databases.

If there was no such data for a parent object, we ascertained the type by applying criteria for color indices, which were employed to select quasars in [Glikman et al., 2018, 2022]. The color indices are determined from WISE photometric data.

For the weakest optical objects, we analyzed cutouts from the WISE survey. If an object was bright in the W1 and W2 bands, but absent in the W3 and W4 bands, we classified it as a galaxy. If the object remained bright in the W3 and W4 bands, we assigned it to quasars.

As a result, we have divided the parent objects into galaxies, quasars, and galaxies with an IR excess. For the last ones, the color indices correspond to the color indices of quasars according to the WISE photometry, but the objects themselves are not classified as stellar in optical surveys. In the sample, the percentage of parent objects by type were: galaxies — 73 %, quasars — 12 %, galaxies with an IR excess — 15 %. Note for comparison that among the parent objects of GRS galaxies account for 82 % by Dabhade et al. [2020] and 80 % by Kuzmicz et al. [2018].

4. REDSHIFTS OF PARENT GALAXIES

Of 187 GRS, 95 have spectral redshifts; 77, photometric ones; and there is no information on redshifts for 15.

To estimate redshifts of parent galaxies of GRS, Lara et al. [2001] and Kuzmicz et al. [2018] employ the relationship between apparent stellar magnitudes of the parent galaxies and their redshifts.

Using data on the GRS apparent stellar magnitudes in the r filter, corrected for galactic extinction, and spectroscopic redshifts z, we have plotted a linear relationship between them. The photometric data and spectroscopic redshifts were taken from the PanSTARRS, LS, and SDSS surveys, as well as from the NED and SIMBAD databases.

For 71 galaxies, we derived the following relationship with a correlation coefficient r=0.78 (left panel of Figure):

$$m_r \pm 1.07 = 5.00 \times \log(z) + 21.16,$$

where m_r is the apparent stellar magnitude in the r filter.

We have fitted a separate relationship for quasars. For this purpose, 8 quasars and 15 galaxies were taken which, according to the WISE color index criterion, are classified as quasars. The following relationship was obtained with a correlation coefficient r=0.72 (right panel of Figure):

$$m_r \pm 0.75 = 2.66 \times \log(z) + 19.69.$$

By comparing the spectroscopic redshifts with the values calculated from the formulas, we computed standard deviations of the difference between them, which amounted to 0.07 for galaxies and 0.15 for quasars. Using these relationships, we estimated redshifts of 15 parent objects (12 galaxies and three quasars).

The median value of redshifts was 0.14 for 95 objects with spectroscopic redshifts, 0.30 for 77 objects

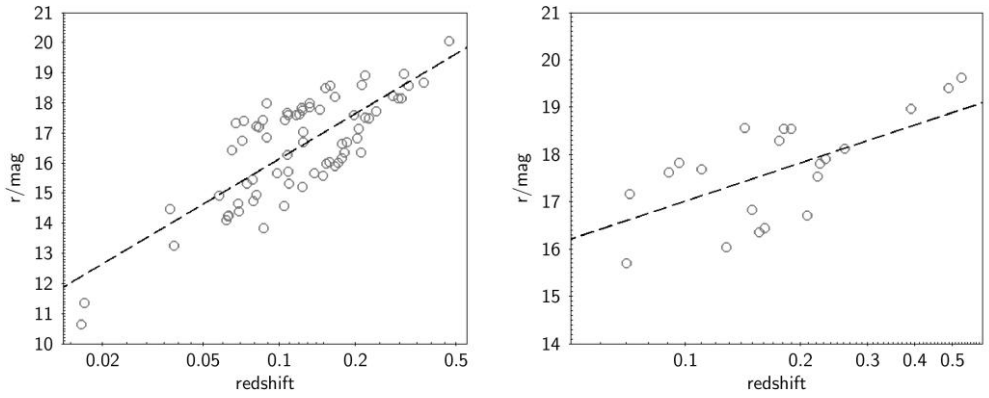

Scatter plots of points for apparent stellar magnitudes m_r and spectroscopic redshifts z of GRS parent objects: on the left — for 71 giant radio galaxies, on the right — for 23 giant radio quasars. The X-axis is plotted on a logarithmic scale

with photometric redshifts, 0.61 for 15 objects with redshifts estimated from the obtained relationships.

5. RADIO MORPHOLOGY

We have morphologically classified GRS from NVSS, RACS, FIRST, and VLASS survey maps. According to NVSS maps, 10 % of the sources were assigned to FRI; 4 %, to FRI/II; and 86 %, to FRII.

In [Kuzmicz et al., 2018], [Dabhade et al., 2020], and [Andernach et al., 2021], the percentage of FRII sources is 90, 89, and 93 % respectively.

We compared the ratio between FRI and FRII sources depending on the redshift for the GRS lists [Kuzmicz et al., 2018; Dabhade et al., 2020] and our sample.

Table 2 presents statistics on four redshift intervals. The list designations are the same as in Table 1. The number of sources is separated by a slash (FRI + FRI/II)/FRII. The last table row shows the mean percentage of FRI+FRI/FRII sources relative to all GRS falling within this redshift interval.

Table 2

Number of FRI+FRI/FRII and FRII sources in redshift intervals

Lists	$z<0.05$	0.05÷0.10	0.10÷0.15	0.15÷0.20
D20	4/7	12/29	20/43	6/37
K18	7/5	13/35	10/34	2/32
OL	3/1	13/13	10/26	1/25
mean	52 %	33 %	28 %	9 %

For close redshifts $z<0.05$, the total number of FRI and FRI/II sources proved to be equal to the total number of FRII sources. However, already at $z=0.05\div0.15$ the number of FRI and FRI/FRII sources decreases markedly, and at $z=0.15\div0.20$ their percentage is only 9 %. Information on the percentage of FRI sources at redshifts $z>0.2$ is not enough.

We suppose that due to the low surface brightness of extended radio lobes, especially in outer regions, it is difficult to detect FRI and FRI/FRII giants already at $z>0.2$. For this reason, their percentage in the GRS lists is generally small.

According to the results of the visual inspection of VLASS maps, we assigned 10 % of GRS to the morphological type Core-Jet/Core-Lobe, (CJ/CL); 13%, to double sources (Double, D); 58%, to double sources with a core (Double-Core, DC); and 20 %, to triple sources (Triple, T). Sources of all the morphological types except D have a core. Thus, 87 % of the sources have a radio core, which allows us to reliably identify parent objects.

Deformation of radio source lobes is an indicator of its environment and/or processes occurring in the immediate vicinity of the active galactic nucleus. For instance, the “tailed” morphology (WAT, Wide-Angle Tailed, or NAT, Narrow-Angle Tailed) indicates that the source is located in a galaxy cluster or group [Owen, Rudnick, 1976; Missaglia et al., 2019]. We have observed this morphological feature in 24 % of GRS in our sample.

The X-, Z-, and S-shaped radio lobes are explained by a change in the orientation of jets caused either by merging of a small galaxy with a massive elliptical parent galaxy, or by accretion disk instability [Dennett-Thorpe et al., 2002; Joshi et al., 2019].

Double radio sources with double lobes (Double-Double, DD) [Brocksopp et al., 2011], as well as triple radio sources [Gopal-Krishna et al., 2012], in which the integral flux density from the radio core is >10 % of the total source flux density, are classified as AGN with jet restart. We have grouped sources with S-, Z-, and X-shaped morphology, as well as DD and T radio sources together, since features of their radio structure indicate processes occurring near the active nucleus. We have found such features in 28 % of the sources.

Half of giants in our sample have one of the morphological features mentioned above or a combination of them.

By comparing NVSS and VLASS maps, we discovered that some sources have radio lobes at 1.4 GHz, yet they are absent or feebly marked on maps at 3 GHz. Thus, we identified radio sources in which the feed of jets had stopped, and they were in the fading phase. There are 74 such sources in our sample.

Given the frequency of occurrence of sources with feebly-marked lobes on VLASS maps, quasars and galaxies with an IR excess have this feature in 16 % of cases; and galaxies, in 47 % of cases.

6. NVRSC-OBJECT VISUAL INSPECTION RESULTS

Of 1616 objects in the NVGRC catalog, we have examined 370 (23 %) within the right ascension interval $00^h00^m < R.A. < 05^h20^m$. We have also studied radio sources with angular sizes of 2.5′ or more, which appeared on radio maps from the NVSS survey of size 1 sq. deg. centered at an NVGRC object.

Some NVGRC objects include components that are not physically connected by the radio sources. There are cases when one component of an NVGRC object belongs to a radio source we classified as GRS, and the other component is not related to the first component. We have identified 18 GRS that fell into the regions in question, but are not included in the NVGRC catalog.

For 187 giants, including NVRSC objects and radio sources that fell into regions of 1 sq. deg. size centered on NVRSC objects, we have obtained the following statistics:

- The parent objects of 70 giant radio galaxies (GRGs) have spectroscopic redshifts, 44 of them are familiar GRGs; and we have discovered 26 new GRGs with four of them omitted from in the NVGRC catalog.
- 55 GRGs have photometric redshifts, 11 of them are included by Dabhade et al. [2020], 44 were confirmed by us, and four of them are left out of the NVGRC catalog.
- 25 giant radio quasars (GRQs) and galaxies with an IR excess have spectroscopic redshifts. We have discovered nine of them with three not included in the NVRSC catalog.
- 22 GRQs have photometric redshifts. We have first identified 16 of them with four omitted from the NVGSC catalog.
- There is no published information on redshifts for 15 parent objects. We have estimated redshifts of these objects, using the relations we obtained between the apparent stellar magnitude and the redshift.

We did not manage to confidently determine the radio structure of seven NVRGC objects: J000106.4+340303, J005451.5+564842, J021329.0+292139(2), J025347.1–200007, J032145.1+514855, J035800.3–393629(2), J050341.2–191142.

Three objects — J011352.3+622434, J043503.2+215527, and J051219.4+131945 — have parent galaxies that are very weak in optics. They are visible only in cutouts of the PanSTARRS survey, but are absent from the PanSTARRS catalog. Their position relative to the radio structure coincides well with the assumed center of the source. Note that sources J011352.3+622434 and J051219.4+131945 are present in the WISE catalog.

78 of 187 GRS have already been classified as giants by Lara et al. [2001], Schoenmakers et al. [2001], Kuzmicz and Jamrozy [2012], Kuzmicz et al. [2018], Dabhade et al. [2020], Oei et al. [2023].

Two NVRSC objects — J005748.3+302114 and J010001.3+300249 — were found to be a single radio source, as were the following NVRSC objects: J022318.0+425939 and J022251.6+425744, J050533.7–285707 and J050540.8–282445, J051601.7+245826 and J051605.7+245833. J024733.6+615632 and J035322.1+355212 are HII regions.

So, among 370 NVGRC objects 169 have been confirmed as GRS. The remaining objects either have sizes less than 0.7 Mpc, or are physically unrelated radio sources that were merged into one radio source by the pattern recognition algorithm.

The sky area we examined using NVSS slices is about 370 sq. deg. The sky area within the right ascension interval from 00^h00^m to 05^h20^m is ~8600 sq. deg. Of the 187 GRS that fell into the surveyed areas, 18 were missed by the pattern recognition algorithm and were omitted from the NVGRC catalog. Hence, the number of objects missed by the algorithm in the specified right ascension interval can be 420. Thus, the efficiency of the pattern recognition algorithm is ~30 %.

CONCLUSION

We have visually examined 370 objects of the NVGRC catalog, which were selected by the pattern recognition algorithm from the NVSS catalog as candidates for giant radio sources, in order to confirm their GRS classification. We have also studied ambient NVSS radio sources in the region of ~1 sq. deg. For 45 % of the examined radio sources, we have confirmed that they belong to GRS, 29 % have sizes less than 0.7 Mpc, and 26 % are independent sources, which were merged into one radio source by the pattern recognition algorithm. In the regions near NVGRC objects, we have found 18 GRS, which are omitted from the NVGRS catalog.

According to VLASS maps, 87 % of GRS have a radio core, which allows us to reliably identify parent objects.

When determining the parent object type, we mainly used information from the SIMBAD and NED databases. If this information was not available for the objects, we applied criteria separating galaxies and quasars according to WISE photometry data. This was mainly employed for objects weak in optics. As a result, our sample of GRS includes 73 % of galaxies, 15 % of galaxies with an IR excess, and 12 % of quasars.

For parent objects with known spectroscopic redshifts, we determined relationships between apparent stellar magnitudes and redshifts both for galaxies and quasars. These relationships were used to estimate redshifts of 15 NVGRC objects for which we could not find redshifts in the databases. With the estimated redshifts, we have confirmed that these objects are GRS.

Of 187 GRS we have confirmed, 78 — 56 galaxies, 16 galaxies with an IR excess, and 6 quasars — were previously known as giants from publications. We have first verified that 109 sources are GRS. For 94 of them, spectroscopic or photometric redshifts of their parent galaxies are known, and for 15 GRS the redshifts were estimated using the m_r–z relationships we have obtained for galaxies and quasars.

Using NVSS maps, we have classified 86 % of sources as FRII, and the rest as FRI and FRI/FRII. We have calculated the number of FRI+FRI/FRII and FRII GRS in four redshift intervals. At $z<0.05$, the percentage of FRI+FRI/FRII and FRII sources was approximately equal, but already at $z>0.15$ the percentage of former decreased

sharply. Thus, the predominance of FRII sources in the GRS lists is most likely associated with the observational selection due to the sensitivity of existing radio surveys.

When comparing NVSS and VLASS maps, we have found that 40 % of the sources can be classified as fading. 25 % of radio sources have a re-started phase. 37 % of sources have deformed radio lobes, indicating that the radio source is located in a galaxy group or cluster. Upon visual examination of optical survey maps, we have observed the presence of close neighbors in some of the parent galaxies of GRS. According to the features of radio morphology and information about redshifts from publications, the neighbors have been found near 121 radio sources. Thus, at least 65 % of GRS are in a fairly dense environment.

The results of the work are presented in Table at [https://www.sao.ru/hq/zhe/ProctorGRSres.txt]. The same file describes columns of the Table.

REFERENCES

Abbott T., Abdalla F., Allam S., et al. The Dark Energy Survey: Data Release 1. *Astrophys. J. Suppl. Ser.* 2018, vol. 239, iss. 2, 18, 25 p. https://doi.org/10.3847/1538-4365/aae9f0.

Aghanim N., Akrami Y., Ashdown M., et al. Planck 2018 results. VI. Cosmological parameters. *Astron. Astrophys.* 2020, vol. 641, A6, 67 p. https://doi.org/10.1051/0004-6361/201833910.

Ahumada R., Allende P., Almeida A., et al. The 16th data release of the Sloan Digital Sky Surveys: First release from the APOGEE-2 Southern Survey and full release of eBOSS spectra. *Astrophys. J. Suppl. Ser*. 2020, vol. 249, iss. 1, 3. https://doi.org/10.3847/1538-4365/ab929e.

Andernach H., Jiménez-Andrade E., Willis A. Discovery of 178 giant radio galaxies in 1059 deg^2 of the Rapid ASKAP Continuum Survey at 888 MHz. *Galaxies.* 2021, vol. 9, iss. 4, 99.? https://doi.org/10.3390/galaxies9040099.

Bonnarel F., Fernique P., Bienaymé O., et al. The ALADIN interactive sky atlas. A reference tool for identification of astronomical sources. *Astron. Astrophys. Suppl.* 2000, vol. 143, p. 33–40. https://doi.org/10.1051/aas:2000331.

Brocksopp C., Kaiser C., Schoenmakers A., et al. Double-double radio galaxies: further insights into the formation of the radio structures. *MNRAS.* 2011, vol. 410, iss. 1, pp. 484–498. https://doi.org/10.1111/j.1365-2966.2010.17456.x.

Chambers K., Magnier E., Metcalfe N., et al. The Pan-STARRS1 Surveys. *eprint arXiv*: 1612.05560, 2016, 38 p. https://doi.org/10.48550/arXiv.1612.05560.

Condon J., Cotton W., Greisen E., et al. The NRAO VLA Sky Survey. *Astronom. J.* 1998, vol. 115, iss. 5, pp. 1693–1716. https://doi.org/10.1086/300337.

Dabhade P., Gaikwad M., Bagchi J., et al. Discovery of giant radio galaxies from NVSS: radio and infrared properties. *MNRAS*. 2017, vol. 469, iss. 3, pp. 2886–2906. https://doi.org/10.1093/mnras/stx860.

Dabhade P., Mahato M., Bagchi J., et al. Search and analysis of giant radio galaxies with associated nuclei (SAGAN). I. New sample and multi-wavelength studies. *Astron. Astrophys.* 2020, vol. 642, A153, 31 p. https://doi.org/10.1051/0004-6361/202038344.

Dennett-Thorpe J., Scheuer P., Laing R., et al. Jet reorientation in active galactic nuclei: two winged radio galaxies. *MNRAS*. 2002, vol 330, iss. 3, pp. 609–620. https://doi.org/02.05106.x 10.1046/j.1365-8711.20.

Dey A., Schlegel D., Lang D., et al., Overview of the DESI Legacy Imaging Surveys. *Astronom. J.* 2019, vol. 157, iss. 5, 168, 29 p. https://doi.org/10.3847/1538-3881/ab089d.

Enßlin T., Gopal-Krishna. Are cluster radio relics revived fossil radio cocoons? *Particles and Fields in Radio Galaxies Conference, ASP Conf. Proc.* 2001, Vol. 250. p. 454. https://doi: https://doi.org/10.1051/0004-6361:20000198.

Fanaroff B., Riley J. The morphology of extragalactic radio sources of high and low luminosity. *MNRAS.* 1974, vol. 167, pp. 31–36. https://doi.org/10.1093/mnras/167.1.31P.

Glikman E., Lacy M., LaMassa S., et al. Luminous WISE-selected obscured, unobscured, and red quasars in Stripe 82. *Astrophys. J.* 2018, vol. 861, iss. 1, 37, 27 p. https://doi.org/10.3847/1538-4357/aac5d8.

Glikman E., Lacy M., La Massa S., et al. The WISE-2MASS Survey: Red quasars into the radio quiet regime. *Astrophys. J.* 2022, vol. 934, iss. 2, 119, 24 p. https://doi.org/10.3847/1538-4357/ac6bee.

Gopal-Krishna, Biermann P., Gergely L., et al. On the origin of X-shaped radio galaxies. *Res. Astron. Astrophys*. 2012, vol. 12, iss. 2, pp. 127–146. https://doi.org/10.1088/1674-4527/12/2/002.

Hardcastle M., Cheung C., Feain I., et al. High-energy particle acceleration and production of ultra-high-energy cosmic rays in the giant lobes of Centaurus A. *MNRAS.* 2009, vol. 393, iss. 3, pp. 1041–1053. https://doi.org/10.1111/j.1365-2966.2008.14265.x.

Helou G., Madore B., Schmitz M., et al. The NASA/IPAC Extragalactic Database. *Information & On-Line Data in Astronomy*. 1995, p. 95. (Astrophys. Space Sci. Library, vol. 203). https://doi.org/10.1007/978-94-011-0397-8_10.

Joshi R., Krishna G., Yang X., et al. X-shaped radio galaxies: Optical properties, large-scale environment, and relationship to radio structure. *Astrophys. J.* 2019, vol. 887, iss. 2, 266, 13 p. https://doi.org/10.3847/1538-4357/ab536f.

Kaiser C., Dennett-Thorpe J., Alexander P. Evolutionary tracks of FRII sources through the P-D diagram. *MNRAS.* 1997, vol. 292, iss. 3, pp. 723–732. https://doi.org/10.1093/mnras/292.3.723.

Komberg B., Pashchenko I. Giant radio galaxies: Old long-lived quasars? *Astronomy Reports*. 2009, vol. 53, iss. 12, pp. 1086–1100. https://doi.org/10.1134/S1063772909120026.

Kronberg P. Extragalactic magnetic fields. *Reports on Progress in Physics*. 1994, vol. 57, iss. 4, pp. 325–382. https://doi.org/10.1088/0034-4885/57/4/001.

Kronberg P., Dufton Q., Li H., et al. Magnetic energy of the intergalactic medium from galactic black holes. *Astrophys. J.* 2001, vol. 560, iss. 1, pp. 178–186. https://doi.org/10.1086/322767.

Kronberg P., Colgate S., Li H., et al. Giant radio galaxies and cosmic-ray acceleration. *Astrophys. J.* 2004, vol. 604, iss. 2, pp. L77–L80. https://doi.org/10.1086/383614.

Kuźmicz A., Jamrozy M. Optical and radio properties of giant radio quasars: central black hole characteristics. *MNRAS.* 2012, vol. 426, iss. 2, pp. 851–867. https://doi.org/10.1111/j.1365-2966.2012.21576.x.

Kuźmicz A., Jamrozy M., Bronarska K., et al. An updated catalog of giant radio sources. *Astrophys. J. Suppl. Ser.* 2018, vol. 238, iss. 1, 9, 9 p. https://doi.org/10.3847/1538-4365/aad9ff.

Lara L., Cotton W., Feretti L., et al., A new sample of large angular size radio galaxies. I. The radio data. *Astron. Astrophys*. 2001, vol. 370, pp. 409–425. https://doi.org/10.1051/0004-6361:20010254.

Lawrence A., Warren S. J., Almaini O. The UKIRT Infrared Deep Sky Survey (UKIDSS). *MNRAS.* 2007, vol. 379, iss. 4, pp. 1599–1617. https://doi.org/10.1111/j.1365-2966.2007.12040.x.

Machalski J., Jamrozy M., Zola S., et al. The new sample of giant radio sources. II. Update of optical counterparts, further spectroscopy of identified faint host galaxies, high-

frequency radio maps, and polarization properties of the sources. *Astron. Astrophys.* 2006, vol. 454, iss. 1, pp. 85–94. https://doi.org/10.1051/0004-6361:20054672.

Malarecki J., Jones D., Saripalli L., et al. Giant radio galaxies — II. Tracers of large-scale structure. *MNRAS.* 2015, vol. 449, iss. 1, pp. 955–986. https://doi.org/10.1093/mnras/stv273.

Missaglia V., Massaro F., Capetti A., et al. WATCAT: A tale of wide-angle tailed radio galaxies. *Astron. Astrophys.* 2019, vol. 626, A8, 19 p. https://doi.org/10.1051/0004-6361/201935058.

Mostert R.I.J., Oei M.S.S.L., Barkus B., et al. Constraining the giant radio galaxy population with machine learning and Bayesian inference. *Astron. Astrophys*. 2024, vol. 691, A185, 25 p. https://doi.org/10.1051/0004-6361/202348897.

Ochsenbein F., Bauer P., Marcout J. The VizieR database of astronomical catalogues. *Astron. Astrophys. Suppl.* 2000, vol. 143, p. 23–32. https://doi.org/10.1051/aas:2000169.

Oei M., van Weeren R., Hardcastle,M., et al. The discovery of a radio galaxy of at least 5 Mpc. *Astron. Astrophys.* 2022, vol. 660, A2, 17 p. https://doi.org/10.1051/0004-6361/202142778.

Oei M., van Weeren R., Gast A., et al. Measuring the giant radio galaxy length distribution with the LoTSS, *Astron. Astrophys.* 2023, vol. 672, A163, 41 p. https://doi.org/10.1051/0004-6361/202243572.

Olsen K., Bolton A., Juneau S., et al. The Data Lab: A science platform for the analysis of ground-based astronomical survey data. Astro2020: Decadal Survey on Astronomy and Astrophysics, *Bull. American Astronomical Society*. 2019, vol. 51, iss. 7, 61. https://doi.org/10.48550/arXiv.1903.05130.

Owen F., Rudnick L. Radio sources with wide-angle tails in Abell clusters of galaxies. *Astrophys. J. Lett.* 1976, vol. 205, pp. L1–L4. https://doi.org/10.1086/182077.

Proctor D. A selection of giant radio sources from NVSS. *Astrophys. J. Suppl. Ser*. 2016, vol. 224, iss. 2, 18, 13 p. https://doi.org/10.3847/0067-0049/224/2/18.

Safouris V., Subrahmanyan R., Bicknell G.V., et al. MRCB0319-454: probing the large-scale structure with a giant radio galaxy. *MNRAS.* 2009, vol. 393, iss. 1, pp. 2–20. https://doi.org/10.1111/j.1365-2966.2008.14181.x.

Schoenmakers A., de Bruyn A., Röttgering H., et al. A new sample of giant radio galaxies from the WENSS survey. I. Sample definition, selection effects and first results. *Astron. Astrophys*. 2001, vol. 374, pp. 861–870. https://doi.org/10.1051/0004-6361:20010746.

Solovyov D., Verkhodanov O. Search for and study of weak radio galaxies with large angular sizes using the NVSS data. *Astronomy Reports*. 2014, vol. 58, iss. 8, pp. 506–515. https://doi.org/10.1134/S106377291408006X.

Taylor M. TOPCAT & STIL: Starlink Table/VOTable Processing Software. *ADASS XIV ASP Conf. Ser.* 2005, Vol. 347, p. 29.

Vallenari A., Brown A. Gaia Data Release 3. Summary of the content and survey properties. *Astron. Astrophys*. 2023, vol. 674, A1, 22 p. https://doi.org/10.1093/mnras/167.1.31P.

van Weeren R., Röttgering H., Brüggen M., et al. Particle acceleration on megaparsec scales in a merging galaxy cluster. *Science*. 2010, vol. 330, iss. 6002, p. 347. https://doi.org/10.1007/s11214-019-0584-z.

Verkhodanov O., Solovyov D., Ulakhovich O., et al. A comparison of properties of different population radio galaxies based on the Planck mission microwave data. *Astrophys. Bull.* 2016, vol. 71, iss. 2, pp. 139–150. https://doi.org/10.1134/S1990341316020024.

Wenger M., Ochsenbein F., Egret D. The SIMBAD Astronomical Database. The CDS Reference Database for astronomical objects. *Astron. Astrophys. Suppl.* 2000, vol. 143, p. 9–22. https://doi.org/10.1051/aas:2000332.

Wright E., Eisenhardt P., Mainzer A., et al. The Wide-field Infrared Survey Explorer (WISE): Mission description and initial on-orbit performance. *Astronomical J.* 2010, vol. 140, iss. 6, pp. 1868–1881.https://doi.org/10.1088/0004-6256/140/6/1868.

URL: https://www.sao.ru/hq/zhe/ProctorGRSres.txt (access February 10, 2026).

Original Russian version: Zhelenkova O.P., Khoruzhenko M.V., published in Solnechno-zemnaya fizika. 2026, vol. 12, no. 2, pp. 97–104. https://doi.org/10.12737/szf-122202610.

How to cite this article

Zhelenkova O.P., Khoruzhenko M.V. Analysis of giant radio source candidates based on multiwavelength data. *Sol.-Terr. Phys.* 2026, vol. 12, iss. 2, pp. 89–95. https://doi.org/10.12737/stp-122202610